1997

Control of Flow Separation Using Adaptive Airfoils

Chandrasekhara, M.S.; Wilder, M.C; Carr, L.W.

M.S. Chandrasekhara, M.C. Wilder and L.W. Carr, "Control of Flow Separation Using Adaptive Airfoils ", AIAA Paper 97-0655, Reno, NV, Jan.1997.
https://hdl.handle.net/10945/50036

AIAA Meeting Papers on Disc, January 1997
A9715684, AIAA Paper 97-0655

Control of flow separation using adaptive airfoils

M. S. Chandrasekhara
U.S. Naval Postgraduate School, Monterey, CA

M. C. Wilder
MCAT, Inc., San Jose, CA

L. W. Carr
NASA, Ames Research Center, Moffett Field, CA

AIAA, Aerospace Sciences Meeting & Exhibit, 35th, Reno, NV, Jan. 6-9, 1997

A novel way of controlling compressible flow separation, using a dynamically deforming leading edge airfoil whose nose curvature can be changed by 400 percent to keep the flow attached at post-stall angles of attack is reported. The strong fluid acceleration around the airfoil nose and the resulting steep adverse pressure gradient were reduced by progressively rounding the airfoil leading edge. Steady flow studies at M = 0.3 showed that the flow separating at about 14 deg angle of attack over a NACA 0012 airfoil could be kept attached up to about 18 deg by increasing the nose radius. Also, a fully separated flow at high angles could be made to reattach by rounding the leading edge. Interestingly, the flow over an airfoil having a nearly semicircular nose was separated even at low angles. The research showed that a 'window' of angles of attack and airfoil profiles exists in which it appears possible to keep the flow attached through a maneuver. The shape change also modified the multiple shocks that form over the NACA 0012 airfoil at M = 0.45. Significant effects of shape change were observed on the vorticity flux in the flow. (Author)

Control of Flow Separation Using Adaptive Airfoils

M.S. Chandrasekhara[1]
Navy-NASA Joint Institute of Aeronautics
Department of Aeronautics and Astronautics
Naval Postgraduate School, Monterey, CA 93943

M.C. Wilder[2]
Navy-NASA Joint Institute of Aeronautics and
MCAT Inc., San Jose, CA

and

L.W. Carr[3]
Aeroflightdynamics Directorate, Aviation Research, Development and
Engineering Center, U.S.Army ATCOM and,
Fluid Mechanics Laboratory Branch
NASA Ames Research Center, Moffett Field, CA 94035-1000

Abstract

A novel way of controlling compressible flow separation, using a dynamically deforming leading edge airfoil whose nose curvature can be changed by 400% to keep the flow attached at post-stall angles of attack is reported. The strong fluid acceleration around the airfoil nose and the resulting steep adverse pressure gradient were reduced by progressively rounding the airfoil leading edge. Steady flow studies at M = 0.3 showed that the flow separating at about 14 degrees angle of attack over a NACA 0012 airfoil could be kept attached up to about 18 degrees by increasing the nose radius. Also, a fully separated flow at high angles could be made to reattach by rounding the leading edge. Interestingly, the flow over an airfoil having a nearly semicircular nose was separated even at low angles. The research showed that a "window" of angles of attack and airfoil profiles exists in which it appears possible to keep the flow attached through a maneuver. The shape change also modified the multiple shocks that form over the NACA 0012 airfoil at M = 0.45. Significant effects of shape change were observed on the vorticity flux in the flow.

Nomenclature

C_l	lift coefficient
C_p	pressure coefficient
$C_{p_{min}}$	peak suction pressure coefficient
c	airfoil chord
f	frequency of oscillation, Hz
k	reduced frequency $= \frac{\pi f c}{U_\infty}$
M	freestream Mach number
U_∞	freestream velocity
Re	Reynolds number based on chord
s,n	distance along and normal to surface
x,y	chordwise and vertical distance
α	angle of attack
ν	kinematic viscosity
Ω	z-component of vorticity
ρ	fluid density

[1]**Associate Director and Research Professor; Associate Fellow, AIAA.** *Mailing Address: M.S. 260-1. NASA Ames Research Center, Moffett Field, CA 94035*

[2]**Sr. Research Scientist, Member AIAA**

[3]**Research Scientist and Group Leader, Unsteady Viscous Flows, Member AIAA**

1. Introduction

It is well known that performance of aircraft and their components is severely restricted by the occurrence of flow separation.Therefore, it will be necessary to control and manage flow separation over airfoils and wings if sustained high lift conditions are expected. The problem is even more important in unsteady flows such as encountered over the retreating blade of a helicopter rotor, a pitching aircraft wing or a wing subjected to gust loads. A review of available literature shows that a popular method for control of flow separation is use of acoustic excitation[1,2]. Ahuja and Burrin[1] used high intensity sound to maintain attached flow over a NACA 65(1)-213 airfoil for about 3 degrees beyond the unexcited static stall angle. However, a very high sound level, of about 150 dB, was needed. Zaman and McKinzie[2] manipulated the laminar separation by acoustic excitation in the Reynolds number range $2.5 \times 10^4 \leq Re \leq 1.0 \times 10^5$. Another method of delaying separation that is commonly used is suction and/or blowing. Generally a very high blowing coefficient is needed for this method to succeed. However, Seifert et al.[3] utilized oscillatory blowing with essentially zero net mass flux and achieved considerable success in delaying trailing edge flow separation. It is worth noting here that all such previous efforts, except oscillatory blowing, are limited to incompressible speeds.

The task of flow control becomes more complicated in compressible and unsteady flows. It is very important to first determine the cause of flow separation in such flows, for the flow can separate due to different mechanisms at different operating conditions as shown by Chandrasekhara et al[4]. Their ongoing research[4,5] on compressibility effects on dynamic stall has demonstrated that dynamic stall onset can arise from:

(1) the bursting of a separation bubble (from the strong adverse pressure gradient downstream of the suction peak) when the flow everywhere is subsonic,

(2) shock induced separation over the airfoil at higher freestream Mach numbers,

(3) a competition amongst these two mechanisms for conditions that are in between.

In addition, both Reynolds number and Mach number play a significant role in the process. The extremely rapid flow acceleration around the airfoil leading edge which is an attribute of the dynamic stall flow, leads to onset of compressibility effects at freestream Mach numbers as low as 0.2, causing premature onset of stall. Thus, if the leading edge flow acceleration and the subsequent development of the adverse pressure gradient are reduced, effective flow control may be achieved. The published literature[6,7] on dynamic stall control describes ideas to revitalize the boundary layer using techniques such as blowing or suction, use of slats and slots, etc. However, the effectiveness of these techniques in unsteady compressible flows remains to be established.

It is clear that if any unsteady compressible flow separation control method is to be effective, it has to address the primary cause of flow separation for all flow conditions encountered by the airfoil. Thus the technique will be required to decrease the strong suction peak values *without* losing the total lift, decrease the steep adverse pressure gradient region (in the present case by widening the suction region over the airfoil). The decrease in peak suction levels will also result in a decrease in compressibility effects and can even result in the elimination of the shocks that otherwise form. These factors prompted the development of the dynamically deforming leading edge (DDLE) airfoil, wherein the airfoil leading edge is deformed to *adapt* to the instantaneous flow conditions in such a way that the flow remains attached throughout the range of angles of attack of interest. As a first test of the concept of use of the deforming leading edge airfoil for flow control, steady flow separation control was attempted. These studies showed that many different flow regimes can result as a consequence of leading edge shape change. This paper describes the first results of this effort.

2. Description of the Experiment

A. Dynamically Deforming Airfoil Leading Edge Design

The dynamically deforming leading edge airfoil is a 6 in. chord airfoil section made in two parts. The first 25% is made from a custom cast, carbon-fiber composite material, built up in several laminations. Its thickness increases progressively from the leading edge where it is about 0.002 in. thick, as shown in Fig. 1. The rear 75% of the airfoil is machined from solid metal, and the leading edge is attached to the rear section by fasteners. The carbon-fiber skin is attached to a mandrel machined to a NACA 0012 profile by a tang (see Fig. 1) cast along with the leading edge. The mandrel is mounted inside the airfoil leading edge section and is connected to two a.c. brushless, computer driven servomotors by a linkage at the quarter-chord-point. This linkage pushes or pulls the airfoil leading edge to produce the required shape change. The mechanism has been designed for controlling two-dimensional compressible dynamic stall of an oscillating airfoil at Mach numbers of up to M = 0.45, and the motors can exert the necessary force (torque) to drive the mandrel at rates of up to 20 Hz to deform the airfoil from its fully extended NACA 0012 shape to a rounded nose in less than 20 millisec. Thus, even with dwell periods in between, the mechanism can change the airfoil leading edge to the required shape and return to the NACA 0012 shape within one pitch oscillation cycle. Encoders mounted on the motors provide exact position information of the mandrel and thus the leading edge. The DDLE airfoil is mounted between two D-shaped windows with L-shaped optical glass inserts, as is schematically shown in Fig. 2, for tests in the compressible dynamic stall facility(CDSF) at NASA Ames Research Center. The details of the facility can be found in Ref. 8. Fig. 3 shows the leading edge curvature changes for shapes 0 to 10 obtained using the present design. The physical displacement of the airfoil leading edge is about 0.003in. ($x/c \approx 0.0005$) for each shape change. In particular, shapes 0, 4, 8 and 10 are shown for which aerodynamic results will be presented later in the figure. The constraint of continuous curvature and slope at the mating point of the DDLE skin and the solid airfoil causes a slight discontinuity at $x/c \approx 0.08$ when the airfoil is fully stretched (shape 0 compared to NACA 0012 shape). Since this point is considerably downstream of the major events of dynamic stall flow, the discontinuity is not expected to adversely influence the flow being studied. The surface of the composite skin is covered with thin plastic tape to remove the effects of any imperfections that may be present due to the fabricating process. Bench tests were conducted to ensure that the deformation is two-dimensional along the span of the DDLE. This was very important to ascertain, especially because other methods of producing a DDLE yielded a strongly three-dimensional shape change (Ref. 9) which is not acceptable for 2-D aerodynamic flow control.

B. Details of the Experiments

These first experiments were carried out in steady flow to prove the concept that a separated flow could be made to reattach by dynamically deforming the leading edge of an airfoil. The Mach number of the experiments ranged from 0.3 to 0.45 in increments of 0.05. The angle of attack was varied from 6 to 20 degrees, with emphasis over the range where the flow was initially separated. The measurement technique used was point diffraction interferometry(PDI), which has been described in detail in Ref. 10 and 11. The control scheme for the brushless motors provides a way to hold the airfoil leading edge at any desired position (i.e. curvature) in order to completely document the flow using PDI during a sweep over a range of angles of attack. Alternatively, the airfoil angle of attack could be set at a fixed value and the leading edge curvature varied. (The controls also permit deforming the airfoil while it is oscillating about a mean angle of attack at specified rates. This latter option has been exercised in dynamic stall tests to be reported in future publications.) PDI images were ob-

tained for several airfoil leading edge curvatures and angles of attack. These were analyzed to determine whether the flow was separated and also to categorize the type of stall that occurred over the airfoil in order to assess the performance of the instantaneous airfoil shape.

The PDI pictures were then processed to obtain the static pressure distributions over the different shapes. By fitting a cubic spline to the pressure distributions, the steady flow surface vorticity flux was calculated using the equation[12]

$$\nu \frac{\partial \Omega}{\partial n} = \frac{1}{\rho} \frac{\partial p}{\partial s}.$$

Also, the lift coefficient over the portion of the airfoil covered in the interferograms ($0 \leq x/c \leq \approx 0.2$) was derived to establish the relative performance of the different airfoil shapes.

C. Uncertainty Estimates

The estimated uncertainties in the data are as follows:

Mach number:	±0.005
angle of attack:	0.05 degrees
reduced frequency:	0.005
C_p:	± 0.1 at M = 0.3
$C_{p_{min}}$:	± 0.5 at M = 0.3
	±0.35 at M = 0.45
$\frac{dC_p}{d(x/c)}$	±25

The uncertainty in C_p depends on the fringe number under consideration and is 1 fringe for the flow in general with about 3 fringes possibly undetectable near the suction peak at M = 0.3. Since the correction for solid and wake blockage was less than 5% for $C_p = -6.0$ at M = 0.3, no corrections were applied to the PDI derived pressures. The gradients were obtained by fitting a spline curve to the pressure distributions and calculating the values at the locations where the pressure values were recorded. The airfoil leading edge displacement was estimated by a calibration procedure for no-flow conditions. Hence, uncertainties are not quoted for the leading edge position with flow over it.

3. Results and Discussion

A. Qualitative Description of Flow at M = 0.3

Figure 4 presents four interferogram images at M = 0.3 for an angle of attack of 18 degrees. The first image is for the fully extended leading edge, shape 0 of the DDLE model. This shape corresponds very closely to the NACA 0012 shape. Although as can be seen from Fig. 3, there are some slight differences between shape 0 and the NACA 0012 shape, the static stall characteristics and pressure distributions are similar, excepting in the region of the laminar separation bubble (see Sec. E). Earlier studies[5] have shown that the NACA 0012 airfoil experiences abrupt leading edge stall by 14 degrees. Similarly, for shape 0, the flow separated from the leading edge at $\alpha = 14$ deg, and hence at $\alpha = 18$ deg, Fig. 4a shows fringes which have clearly departed from the surface. As the nose is retracted at this high angle of attack, the separated flow fully reattaches by shape 9, which can be seen in Fig. 4b. Attached flow is characterized in this image by the density contours following the airfoil nose and turning smoothly parallel to the surface, like streamlines in attached flows. The leading edge has been retracted by only 0.027in., but the curvature change accompanying this movement is sufficient to cause the flow to reattach. The presence of a large number of fringes near the leading edge points to the production of a large suction peak once the flow reattaches. In the third image, Fig. 4c, corresponding to shape 13 and to a leading edge position of 0.0302in. from the baseline leading edge, the fringes over the airfoil appear to have flattened out. Accompanying images at lower angles of attack for this shape show that a laminar bubble forms (which is on the verge of bursting in this image.) Also, the fringes on the downstream side are lifting off the surface, pointing to the possibility of trailing edge stall that may be propagating towards the leading edge. But, since the fringes near the leading edge still follow the "normal" pattern, the airfoil is still developing suction. The flow at this condition appears to be experiencing a mixed-stall behavior with possible trailing edge separation. The last frame Fig. 4d, shape 17, clearly shows leading edge stall once again as the shear layer has separated from the airfoil nose. The airfoil radius of curvature at this condition is large, showing that there is only a range of curvature change that is beneficial.

These images convincingly demonstrate the success of using airfoil leading edge deformation for reattaching separated flow. Similar pictures were obtained at other angles of attack, but it was found that the attached flow region widens as the angle decreases. At higher Mach numbers, the pictures were similar, although the range of shapes through which the DDLE could reattach the flow became smaller with increasing Mach number, as explained in the next section.

B. Airfoil Performance at Different Leading Edge Curvatures

The flow behavior over the airfoil at different angles and leading edge shapes ranging from shape 0 to shape 18 is summarized in Fig. 5a which is a plot of the various flow regimes that appeared in the experiments at M = 0.3. This picture has been drawn from the PDI images in hand, PDI fringe patterns that were observed, but not imaged while conducting the experiments and from the aerodynamic sound that was heard as the flow separated for certain conditions. It is clear that the flow is attached at angles below 8 degrees for all shapes (the shaded area). Static stall occurred at 14 degrees for the NACA 0012 profile. The stall process started as trailing edge stall (increased sound levels, but leading edge flow still attached) accompanied by a general decrease of the peak suction pressure (as measured by a counting of the fringes). In about half-a-degree, the flow reached the leading edge stall state. Essentially the same trend was observed for shape 0. That trailing edge stall occurred could be inferred by examining some of the outer fringes near the 20% chord point which had

begun to lift away from the surface, whereas the inside fringes were all regular. No significant changes in the flow were noticed until the nose was pulled back to shape 8. For the leading edge position corresponding to shape 8, (the change in the radius of curvature is estimated to be about 100% higher than the NACA 0012 nose radius) the flow remained attached up to an angle of attack of 18 degrees.

For all shapes a laminar separation bubble was present in the attached flow cases, just as was seen for the NACA 0012 airfoil. A noticeable effect of decreasing the nose curvature at post-stall angles of attack was the sudden decrease in the audible tunnel sound as soon as the flow reattached. For shape 8, the flow began to separate at $\alpha = 19$ deg. Thus, the tunnel flow was quiet over angles of attack from 0 - 18 degrees. However, as the pressure distributions presented later will show, the suction peak decreased gradually. Beyond $\alpha = 12$ deg, the bubble appeared to open up into an organized structure around x/c = 0.06 - 0.08 for shapes 10 through 14, but the outer flow was still attached over the airfoil further downstream before trailing edge stall started. This flow regime is termed "mixed flow" in this article. As the leading edge was retracted further, the flow abruptly stalled from the leading edge. Interestingly, as a semicircular nose shape was approached, the flow began to experience leading edge stall at *much* lower angles of attack when compared to the NACA 0012 profile. Thus, it appears that a "window" of airfoil shapes is present at post-stall angle of attack conditions in which the flow remains attached or can be made to reattach if it has already separated. Outside this window, the flow conditions degrade rapidly. A similar flow regime map has been drawn for M = 0.35 in Fig. 5b and in Fig. 5c for M = 0.45. The major difference seen is a decrease in angles of attack at which the above mentioned regimes occur and also a much narrower window of airfoil shapes where quasi-steady flow control can be successfully attained with increase in Mach number. This window provides a new and extended flight envelope for a wing to maneuver by constantly pursuing the "right" airfoil shape if its angle of attack is increased beyond the static stall angle.

The flow patterns observed for M = 0.45 in steady flow show that the baseline profile stalled at about 11 degrees. However, as the nose radius of curvature was increased, the flow could be made to stay attached up to $\alpha \approx 12 - 13$ deg. But, as the nose became more rounded, the flow separated from x/c = 0.08 - 0.1. Still, the airfoil continued to develop suction with increasing angle of attack. However, the separation propagated upstream and eventually caused leading edge stall. Another noteworthy point here is the presence of a series of shocks for most of the attached flow cases for the angles of attack shown. In the mixed flow region, a structure as described for M = 0.3 was not present, the overall flow was still attached and the suction pressure was large, but the shocks may have induced mild local separation.

C. Development of Suction Peak for Different Shapes

Figure 6a presents the development of peak suction at M = 0.3 for shapes 0, 4, 8, and 10 (progressively increasing nose radius) along with the data for NACA 0012 shape. It shows that the NACA 0012 profile developed slightly higher suction levels when compared to shape 0. However, when this figure is interpreted in conjunction with Fig. 5a for M = 0.3, it seems that by carefully shaping the airfoil from the baseline profile to shape 8 for angles of attack from 14 - 18 degrees, the airfoil can be steadily made to produce significant lift. Even though the suction peak drops for shape 8, it is believed that the increase in drag due to the high angle of attack is not significant, because the flow is fully attached. The highest $C_{p_{min}}$ value is about -6.5 for shapes 8 and 10 which is slightly less than that observed for the NACA 0012 profile. Most importantly, the suction produced decreases progressively with increasing nose radius at any given angle up to $\alpha = 14$ deg and the development of a given peak suction level is delayed to higher angles by the rounding of the nose. This points to the fact that the flow acceleration is reduced with increasing leading edge radius, offering a reliable means of reducing the compressibility effects that otherwise set in this flow.

Data for M = 0.45 presented in Fig. 6b show that at a given angle of attack, rounding the nose produces a lower suction at the same angle of attack up to 10 degrees. Once again, there is not much difference between the NACA 0012 shape and DDLE shape 0 values. The fall of the peak suction is more gradual in case of shape 0, possibly due to trailing edge stall. The flow is supersonic for all shapes at the suction peak location. But, since the decreasing suction peak values cause lower local supersonic velocities as the airfoil nose is rounded, the system of shocks that forms is weaker with increasing leading edge radius. It is also interesting to note that at M = 0.45, a narrow range of DDLE shape changes (from 1-4) produces dramatic changes in the flow development, unlike that at M = 0.3, where a larger window (shapes from 1-10) is available. Further, the leading edge curvature for shape 5 and higher degrades the flow considerably. Despite the higher suction levels that are produced at $\alpha \geq 10$ deg, it may not be desirable to reach these angles, since the objective is to minimize the effects of shocks that form at this Mach number. Nevertheless, about 2 degrees of delay in stall onset conditions is achieved for M = 0.45 by using a deforming leading edge airfoil. From such a parametric study, it would be possible to derive an "optimal" shape history for each Mach number and used as the different flight conditions warrant. This history is still to be determined.

D. Description of Flow Over Shape 8 at M = 0.3

Figures 7 a-c show representative interferograms at $\alpha = 10.0$ deg, 13.99 deg and 18.0 deg for shape 8. As is well known, the fringes are contours of constant density and in isentropic flow, also correspond to constant pressure contours. The surface pressure distributions from these images and two other angles are included in Fig. 7d. As the flow accelerates from the stagnation point on the lower surface in Fig. 7a, a suction peak develops, which is marked on the upper surface by the fringe that encloses no other fringe.

Two fringes above it, some fringes level off slightly downstream and meet the surface almost vertically. This can be seen more clearly in Fig. 7b. Earlier research[10] has shown that this fringe pattern corresponds to a laminar separation bubble, a fact also borne out by the pressure distributions in Fig. 7d. Fig. 7c shows the bubble still attached at $\alpha = 18$ deg although the outer fringes have begun to lift off the surface. Since no distinctive sound change was audible, it is believed that the flow is still attached over the airfoil. The reduced peak suction level at this high angle is attributed to the large wake width in such flow, which increases the viscous/inviscid interaction considerably. The bubble in this flow is about 4% chord long compared to about 2% chord long in the NACA 0012 airfoil flow.

E. Surface Pressure Distributions Over Different DDLE Shapes

Figure 8a shows the pressure distributions obtained from the interferograms for the NACA 0012 shape and shape 0; Fig. 8b and 8c show these for shapes 4 and 10. Although the NACA 0012 profile is very nearly identical to shape 0, there are some differences between the corresponding pressure distributions. Whereas most of the differences are almost within the experimental uncertainty, the C_p values over the NACA 0012 are slightly more negative than those for shape 0. A more noticeable difference in each of the profiles is present in the plateau that corresponds to the laminar separation bubble. It appears that the bubble forms after a much larger pressure recovery over the shape 0 airfoil. For both shapes, the bubble shrinks as the airfoil angle of attack increases from 7.98 to 12.03 degrees. However, the bubble is longer in the case of DDLE shape 0 at each of the angles of attack compared. Typically for shape 0, the bubble shrinks from about 5% chord length at $\alpha = 7.98$ deg to about 2% chord at $\alpha = 12.03$ deg. The corresponding numbers for the NACA 0012 shape range from about 4% chord to 1.5% chord. The slightly longer bubble would enhance the viscous/inviscid interaction, resulting in slightly reduced suction pressure over this shape. In view of this difference, all further comparisons are made between the various DDLE shapes only.

In Fig. 8b, the $C_{p_{min}}$ value for shape 4 increases as α changes from 10 degrees to 12 degrees, as can be expected. However, the $C_{p_{min}}$ starts decreasing with further increase in angle of attack, and is very low at $\alpha = 18.0$ deg. This trend is consistent with Fig. 5, where trailing edge stall was shown to be present for angles of attack above 14 degrees and leading edge stall at about 16 degrees. As before, a slight decrease in the laminar separation bubble length is observed with increase in airfoil angle of attack.

The distributions for shape 10 show that the flow has already separated at $\alpha = 10.0$ deg. However, it reattaches by 12 degrees and suction develops up to about 14 degrees angle of attack. Subsequently, as trailing edge separation ensues, the leading edge maximum suction falls. The laminar separation bubble forms over this shape as well and is seen to be about 7% chord long at 12.03 degrees angle of attack, shrinking slightly to about 6% chord long at $\alpha = 13.99$ deg.

The above results indicate that the bubble length increases with increasing airfoil leading edge radius, implying that significant fluid dynamics effects are also brought about by this change. It is important to explore the effects of tripping on the flow developments over these shapes and tests are planned in the near future for establishing the associated flow physics.

F. Distributions of Vorticity Fluxes Over Various Shapes

The vorticity fluxes were calculated from the static pressure distributions by taking the derivatives with respect to the distance along the surface. There is considerable noise in the data due to the numerical differentiation used. Even then, when large gradients are involved, the data can quantify the vorticity produced at the surface. As shown by Shih and Ho[13], since the oncoming flow is irrotational, there exists a balance between the continuous production of vorticity at the surface and its convection by the boundary layer fluid. The local production term can be obtained by integrating the gradient $\frac{dC_p}{d(s/c)}$ between any two locations s and $s + ds$. This means that when there is a region of clockwise vorticity over the airfoil, there is vorticity production due to pressure gradient term there, which diffuses outwards. Fig. 9 a-c show the vorticity flux distributions for shapes 0, 4, 8 and 10 for $\alpha = 12.03$, 13.99 and 18 deg respectively. The large value seen in Fig. 9a for shape 0 near the suction peak location ($x/c \approx 0.018$) shows that much of the vorticity for this shape is produced here. Over the bubble region, the production is nearly zero since the gradient is almost zero. (Occasionally, a fringe was found in the bubble region over the different shapes, which resulted in a slight gradient here.) Downstream of the bubble, there is very little vorticity production. In contrast, shape 4 has modest levels of production over the first 10% chord of the airfoil. Interestingly, for shapes 8 and 10, since no suction peak was clearly discernible, much of the production is seen only downstream of the bubble. It is believed that even if a suction peak could be actually detected close to the leading edge for shape 8 and 10, this region would be sufficiently small and hence, its contribution to the total vorticity production would be small, (see Fig. 9b, shape 8 data). Dramatic changes are seen in Fig. 9b for $\alpha = 13.99$ deg, where the vorticity level for shape 0 has fallen substantially from its peak value seen for $\alpha = 10.00$ deg. As explained earlier, shape 0 stalled at around $\alpha = 14$ deg. For shape 4 also, the level has fallen, where as for shapes 8 and 10, there is a large rise at the downstream end of the bubble, spreading out to $x/c = 0.08$. Data presented in Fig. 9c for $\alpha = 18.00$ deg shows zero levels of vorticity for shapes 0 and 4, as can be expected since these airfoils have fully stalled. However, there is still some vorticity being produced by shapes 8 and 10, with a well defined peak in the latter. But, the width of this region has grown smaller. These figures show that deforming the leading edge of the airfoil results in a redistribution of the vorticity flux over the whole airfoil. It seems that in the process, the pressure distributions were significantly modified, altering the stall onset process

and achieving separation control.

G. Distributions of Lift Coefficients for Different Shapes

Figure 10 shows the lift coefficient C_l over the portion of the airfoil for which PDI pressure data is available, plotted against angle of attack. About 20% of the airfoil surface is included in the calculations. The results are compared with the high Reynolds number (4.0×10^6) data of McAlister et al [14] for the same region. The values are higher at the higher Reynolds number. But, it is clear from the figure that progressively more lift was generated by the airfoil as the nose radius was increased at the Reynolds number tested. The increase was also considerable. Shape 8 produced about 30% more lift compared to shape 0 for example. Although the lift coefficient drops as the angle of attack increases beyond 14 degrees, the flow is still attached as shown by the PDI pictures. Thus, it can be said that the deforming leading edge airfoil has successfully been used to control steady separated flow over the airfoil, and the flow control strategy used seems appropriate.

4. Conclusions

A novel concept for control of separation using a deforming leading edge airfoil has been demonstrated in steady compressible flows. These first results show that an initially separated flow can be *made* to reattach by changing the airfoil nose curvature over a range of values and alleviating the local adverse pressure gradient. Also, attached flow can be maintained up to about 18 degrees at M = 0.3 by suitably deforming the airfoil. Deforming the airfoil leading edge alters the distribution of the vorticity flux over the *whole* airfoil and as a consequence, modifies the airfoil pressure distributions such that the flow remains attached up to higher angles of attack. Control seems possible at M = 0.45 even when shocks locally influence the flow considerably. The window of airfoil shapes where flow control is achieved shrinks as the freestream Mach number is increased. Significant fluid physics issues arise as the airfoil nose radius is increased. In particular, the laminar separation bubble size and its effects on the flow are affected at M = 0.3. At M = 0.45, the system of shocks is also affected. More tests to document the influence of Reynolds number, Mach number, degree of unsteadiness, etc. are needed to devise an optimal shape history for such airfoils to sustain attached flow over a range of flow conditions. As the airfoil shape is changed in real-time, significant effects of unsteadiness could develop due to the surface movement involved in the process. The effects of this on the flow vorticity field are yet to be determined, for the different applications in which the DDLE concept may be used.

Acknowledgements

The project was supported by ARO-MIPR-96-7 to the Naval Postgraduate School and was monitored by T.L. Doligalski, with initial funding from AFOSR. Additional support was received from S.S. Davis, Fluid Mechanics Laboratory, NASA ARC. The design and fabrication support of C.D. Sticht, C.Hiel, and G.N. Paulson, the DDLE control system design of D.D. Squires, the help of R.A. Miller in model installation are all greatly appreciated.

References

[1] Ahuja, K.K., and Burrin, R.H., "Control of Flow Separation" *AIAA Paper 84-2298*, Oct. 1984.

[2] Zaman, K.B.M.Q., and McKinzie, D., "Control of Laminar Separation Over Airfoils by Acoustic Excitation", *AIAA Paper 89-0565*, Jan. 1989.

[3] Seifert, A., Bahcar, T., Koss, D., Shepshelovich, M., and Wygnanski, I., "Oscillatory Blowing: A Tool to Delay Boundary Layer Separation", *AIAA Journal*, Vol. 31, No. 11, Oct. 1993, pp. 2052-2060.

[4] Chandrasekhara, M.S., Wilder, M.C., and Carr, L.W., "On the Competing Mechanisms of Compressible Dynamic Stall", *AIAA Paper 96-1953*, Jun. 1996

[5] Chandrasekhara, M.S., Wilder, M.C., and Carr, L.W., "Reynolds Number Influence on 2-D Compressible Dynamic Stall", *AIAA Paper 96-0073*, Jan. 1996.

[6] Alrefai, M. and Acharya, M., "Controlled Leading Edge Suction for the Management of Unsteady Separation over Pitching Airfoils", *AIAA Paper 95-2188*, Jun. 1995

[7] Carr, L.W. and McAlister, K.W., "The Effect of a Leading-Edge Slat on the Dynamic Stall of an Oscillating Airfoil", *AIAA Paper 83-3533*, Oct. 1983.

[8] Carr, L.W., and Chandrasekhara, M.S., "Design and Development of a Compressible Dynamic Stall Facility", *Journal of Aircraft*, Vol. 29, No. 3, pp. 314-318.

[9] Wilder, M.C., "Control of Unsteady Separated Flow Associated with the Dynamic Stall of Airfoils", *Final Report 95-09*, MCAT Institute, San Jose, CA, Jan. 1995.

[10] Carr, L.W., Chandrasekhara, M.S. and Brock, N., "A Quantitative Study of Unsteady Compressible Flow on an Oscillating Airfoil", *Journal of Aircraft*, Vol. 31, No. 4, Jul. - Aug. 1994, pp. 892 - 898.

[11] Chandrasekhara , M.S., and Carr, L.W., "Compressibility Effects on Dynamic Stall of Oscillating Airfoils", *AGARD-CP-552*, Aug. 1995, pp. 3.1 - 3.15.

[12] Reynolds, W.C. and Carr, L.W., "Review of Unsteady, Driven, Separated Flows", *AIAA Paper 85-0527*, Mar. 1985.

[13] Shih, C,, Ho, C.M., "Vorticity Balance and Time Scales of a Two-Dimensional Airfoil in an Unsteady Stream", *Physics of Fluids*, Vol. 6, No. 2, Feb. 1994, pp. 710-723.

[14] McAlister, K.W., Pucci, S.L., McCroskey, W.J., and Carr, L.W., "An Experimental Study of Dynamic Stall on Advanced Airfoil Sections, Vol. 2, Pressure and Force Data", NASA TM-84245, USAAVRAD-COM TR-82-A-8, Sep. 1992.

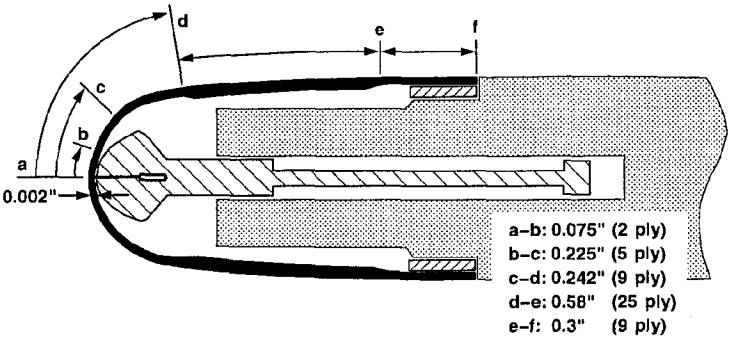

Fig. 1. Construction Details of the DDLE Airfoil Model.

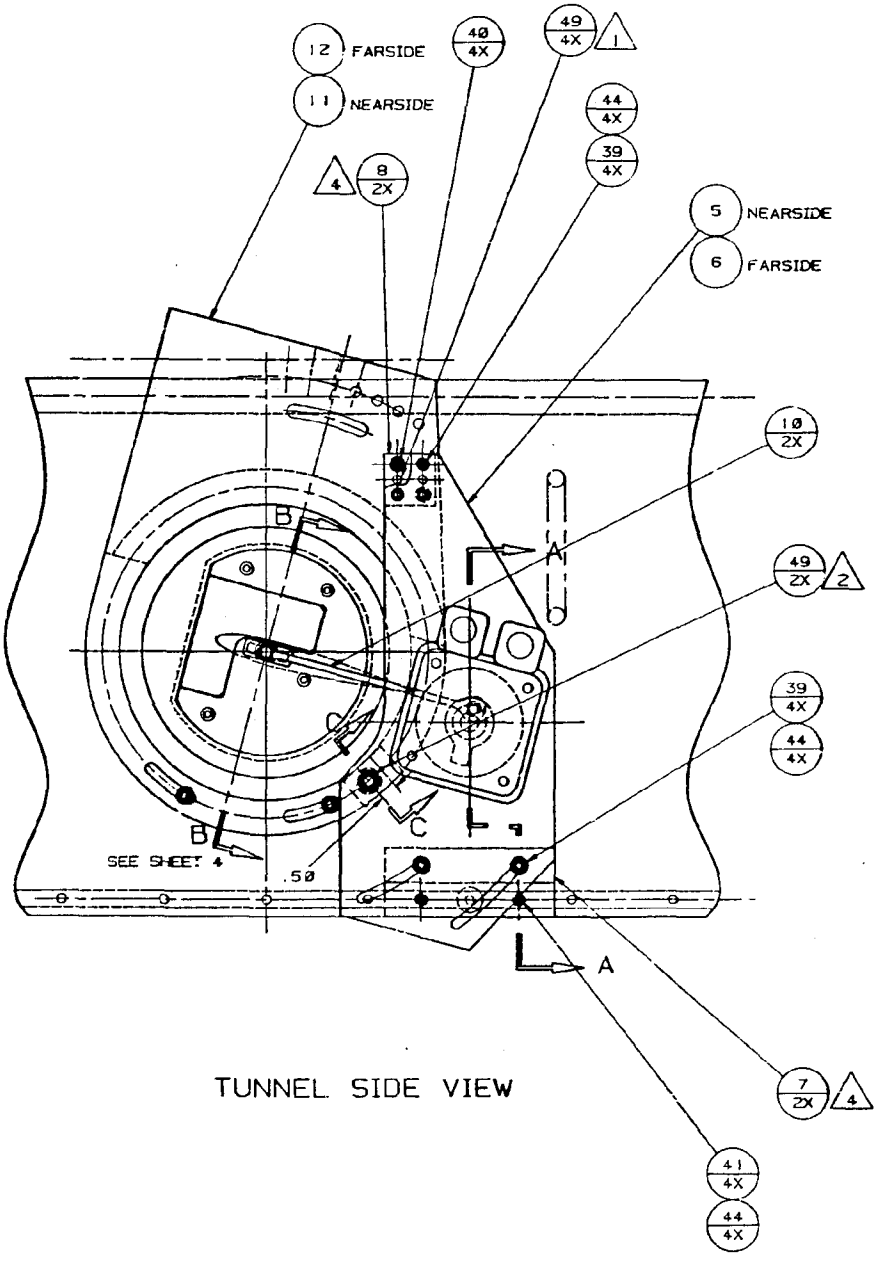

Fig. 2. Schematic of the DDLE Airfoil and Actuator Mechanism.

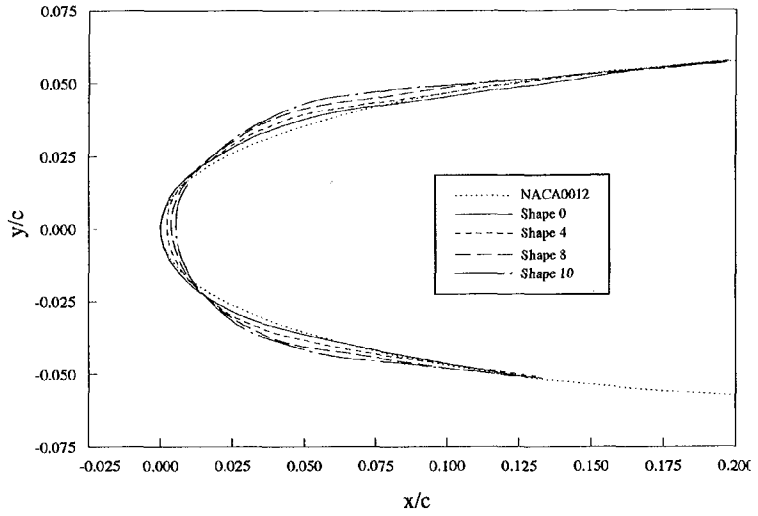

Fig. 3. DDLE Shape Profiles Compared with the NACA 0012 Profile.

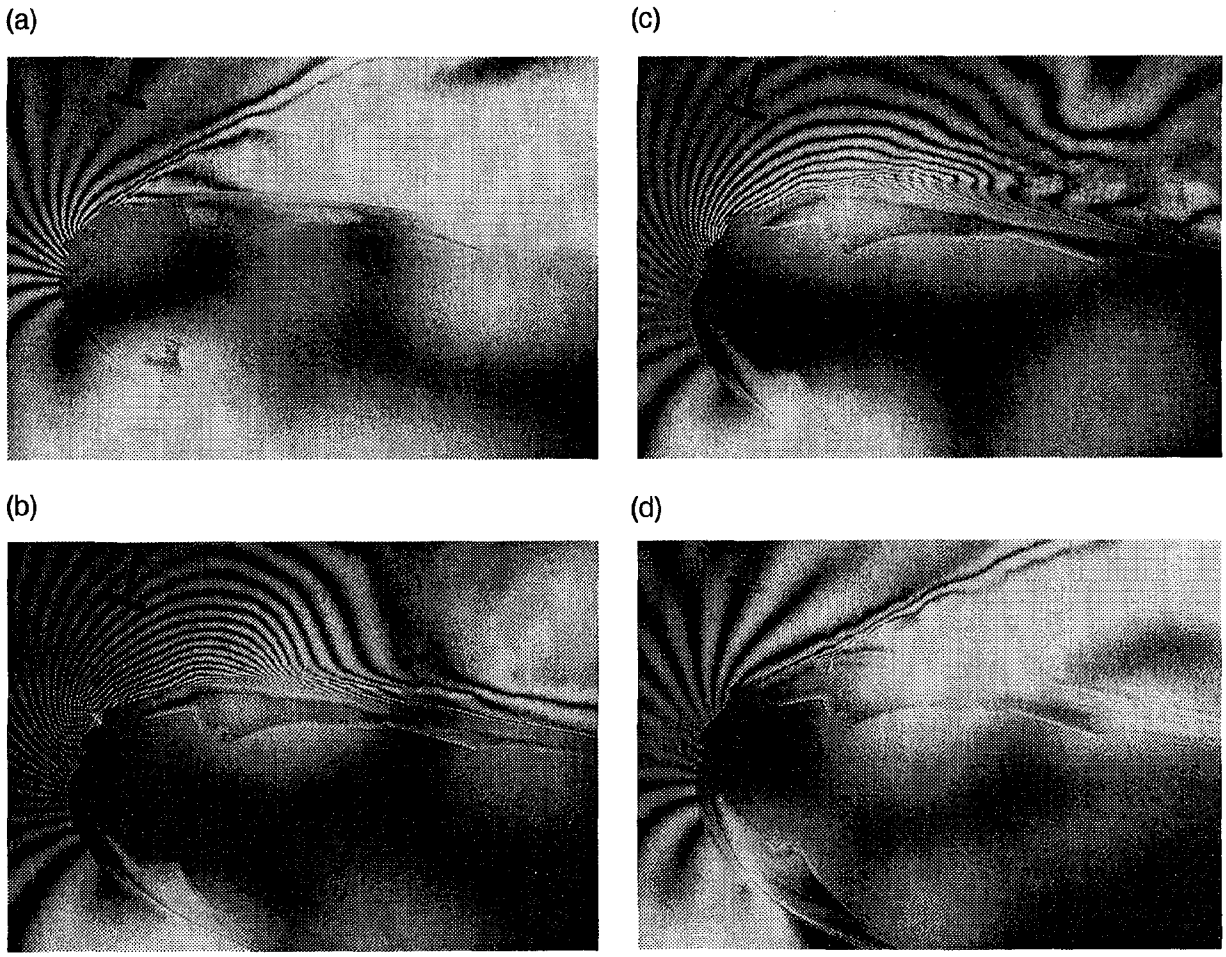

Fig. 4. Flow Modification with Changing Leading Edge Shape, M = 0.3, α = 18.00 deg: (a) Shape 0; (b) Shape 9; (c) Shape 13; (d) Shape 17.

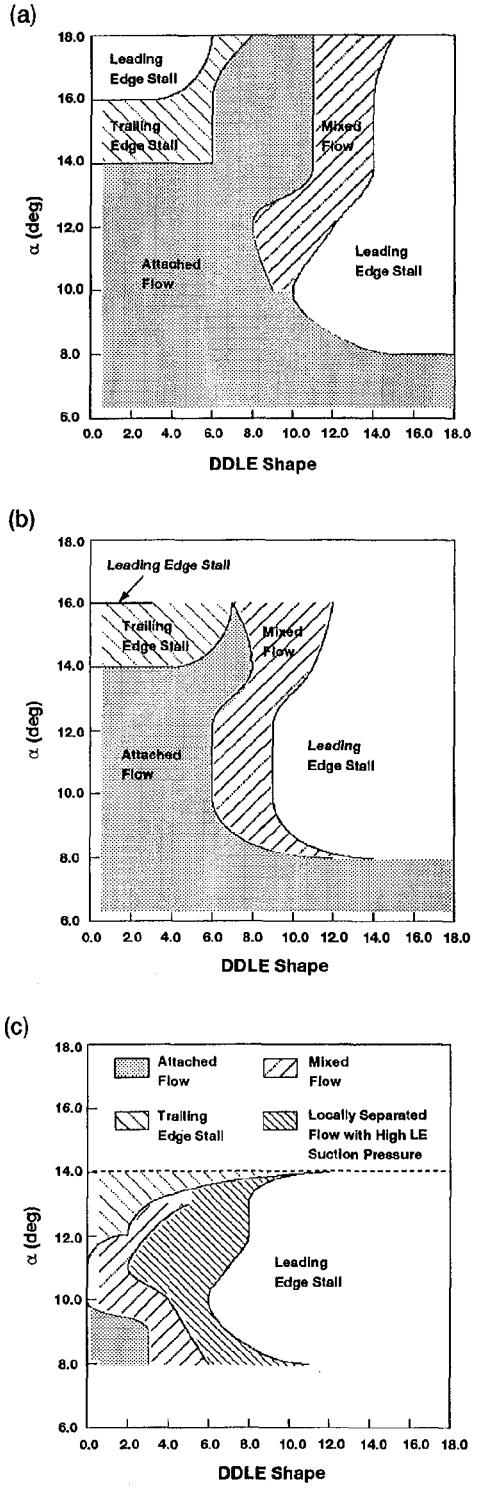

Fig. 5. Flow Regimes for Different Leading-Edge Shapes as a Function of Angle-of-Attack: (a) M = 0.3; (b) M = 0.35; (c) M = 0.45.

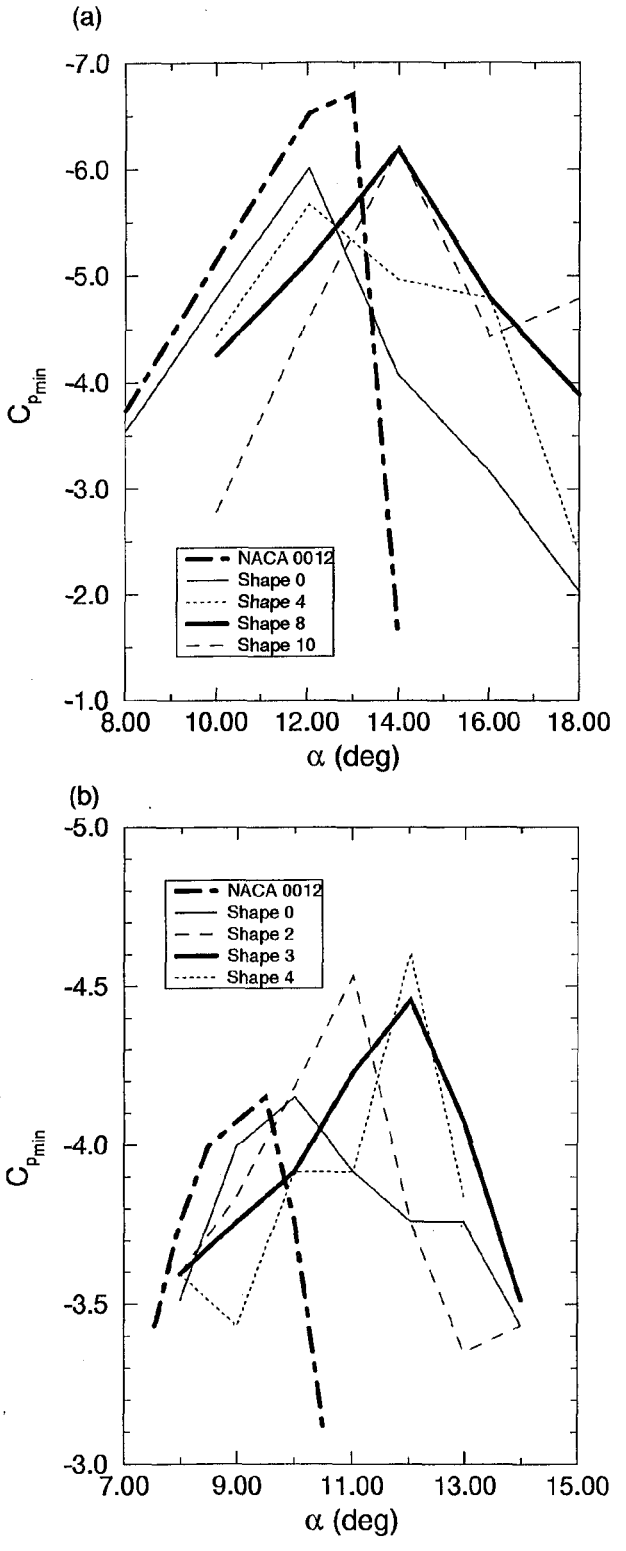

Fig. 6. Development of Peak Suction Pressure Coefficient for Different Leading-Edge Shapes: (a) M = 0.3; (b) M = 0.45.

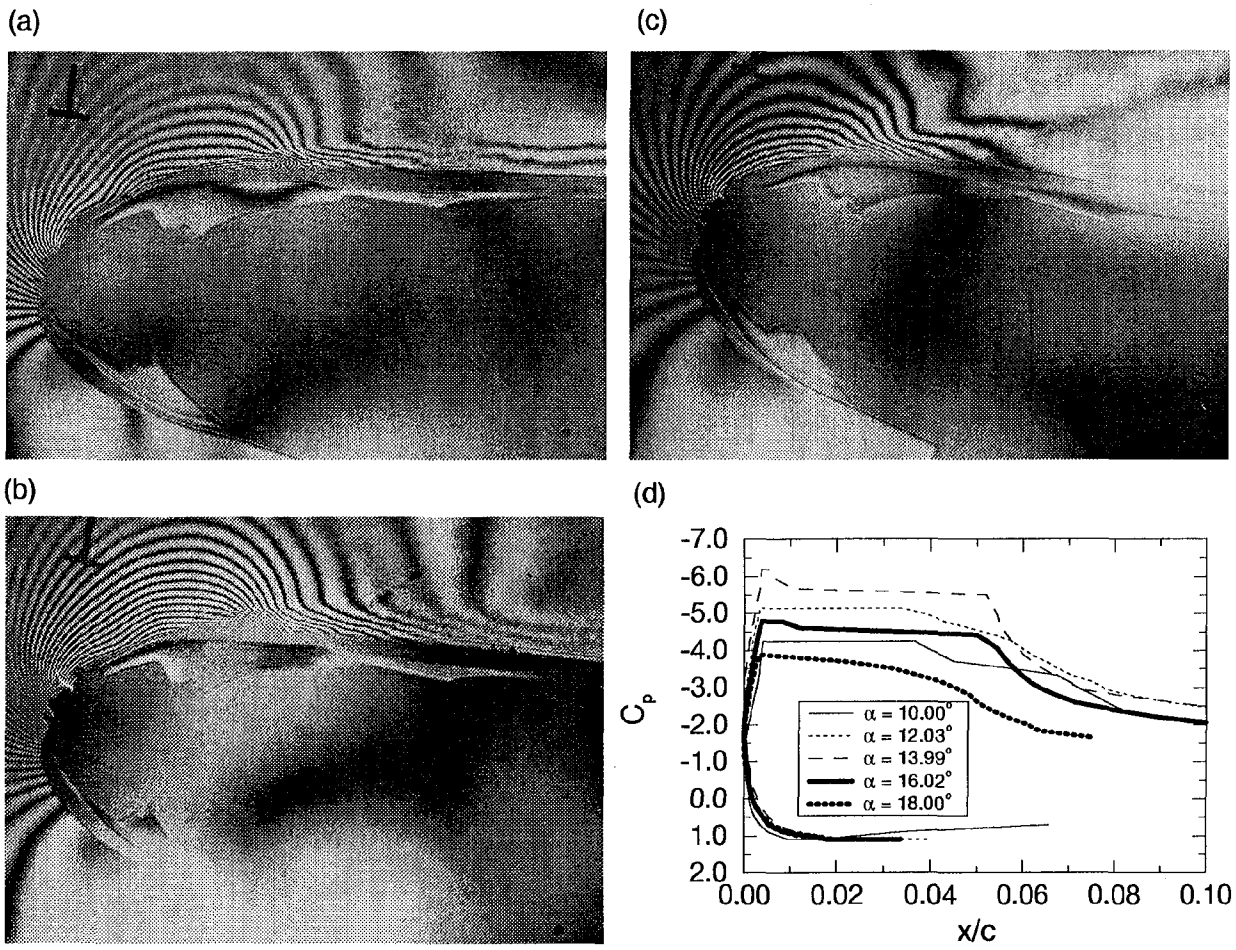

Fig. 7. Flow Development Over Shape 8 Airfoil, M = 0.3: (a) $\alpha = 10.00^{\circ}$; (b) $\alpha = 13.99^{\circ}$; (c) $\alpha = 18.00^{\circ}$; (d) Surface Pressure Distributions.

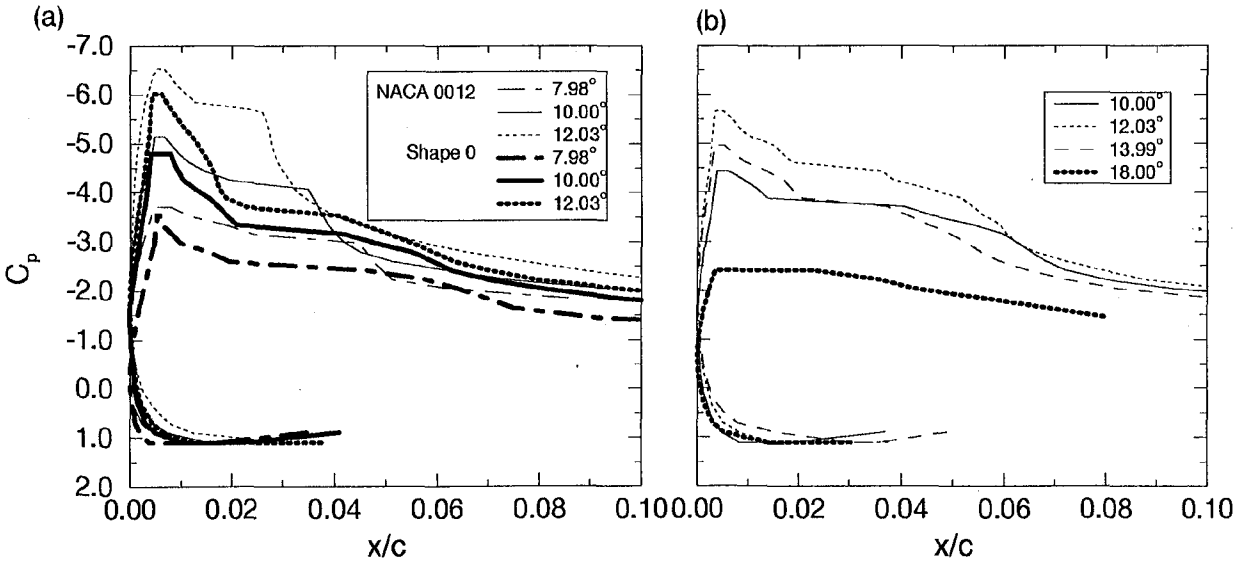

Fig. 8. Surface Pressure Distributions, M = 0.3: (a) NACA 0012 and Shape 0; (b) Shape 4; (cont.)

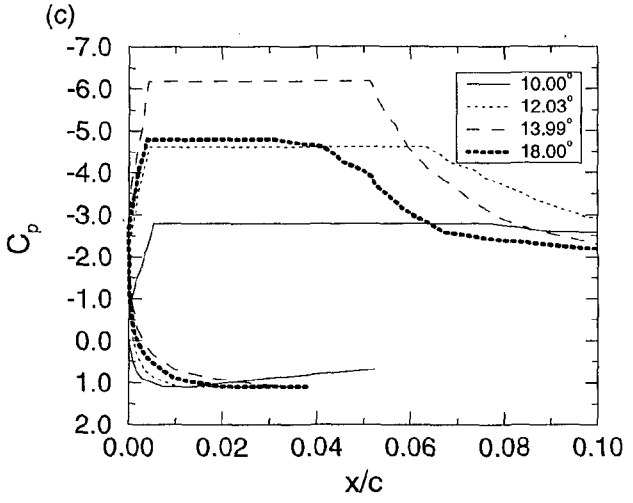

Fig. 8. Surface Pressure Distributions, M = 0.3: (c) Shape 10; (concluded).

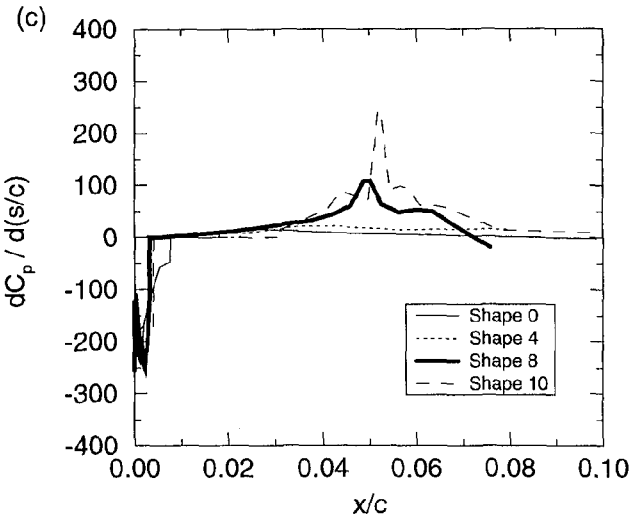

Fig. 9. Vorticity Flux Distributions for DDLE Shapes 0, 4, 8, and 10, M = 0.3: (a) $\alpha = 12.03^{\circ}$; (b) $\alpha = 13.99^{\circ}$; (c) $\alpha = 18.00^{\circ}$.

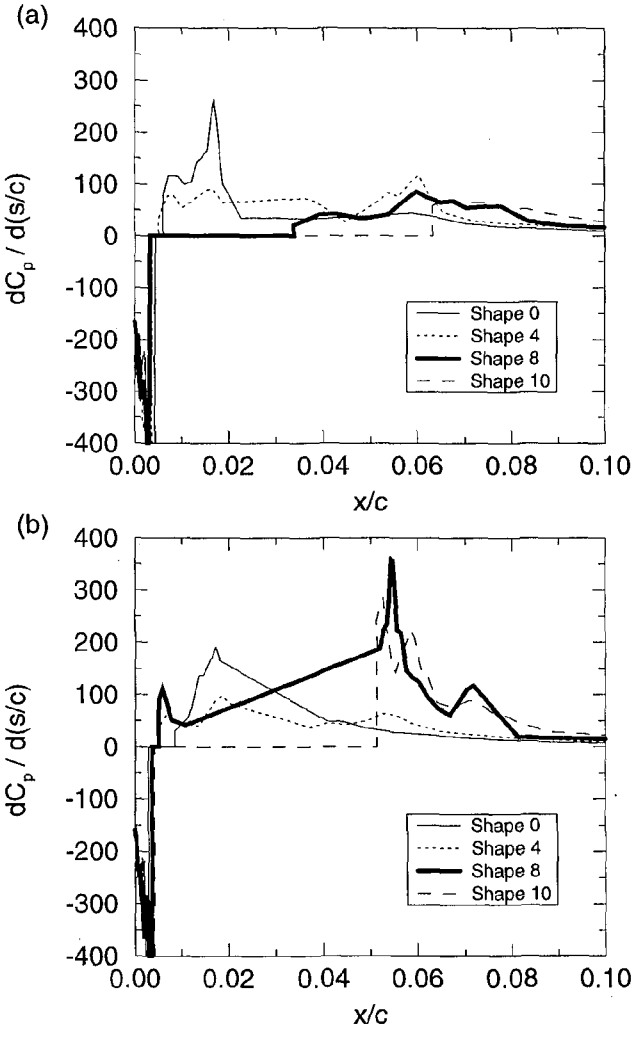

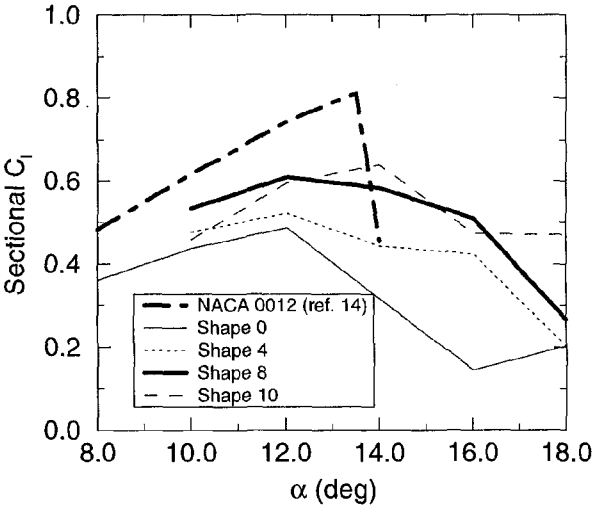

Fig. 10. Development of Sectional Lift Coefficient, M = 0.3.